Groundwater flow and salt transport in a subterranean estuary driven by intensified wave conditions

Clare Robinson,[1] Pei Xin,[2,3] Ling Li,[2,3] and D. A. Barry[4]

[1] A numerical study, based on a density-dependent variably saturated groundwater flow model, was conducted to investigate flow and salt transport in a nearshore aquifer under intensified wave conditions caused by offshore storms. Temporally varying onshore hydraulic gradients due to wave setup were determined as the seaward boundary condition for the simulated aquifer. The results showed a rapid increase in influxes across the aquifer-ocean interface in response to the wave event followed by a more gradual increase in effluxes. The upper saline plume first widened horizontally as the wave setup point moved landward. It then expanded vertically with recirculating seawater pushed downward by the wave-induced hydraulic gradient. The time for the salt distribution to return to the prestorm condition was up to a hundred days and correlated strongly with the time for seawater to recirculate through the aquifer. The pathways of recirculating seawater and fresh groundwater were largely modified by the wave event. These pathways crossed through the same spatial locations at similar times, indicating significant salt-freshwater mixing. The flow and salt transport dynamics were more responsive to wave events of longer duration and higher intensity, especially in more permeable aquifers with lower fresh groundwater discharge. Despite their larger response, aquifers with higher permeability and beach slope recovered more rapidly postevent. The rapid recovery of the flows compared with the salinity distribution should be considered in field data interpretation. Due to their long-lasting impact, wave events may significantly influence the geochemical conditions and the fate of chemicals in a subterranean estuary.

1. Introduction

[2] Submarine groundwater discharge (SGD) from a coastal aquifer provides a significant transport pathway for delivering land-sourced chemicals (e.g., nutrients, pharmaceuticals, and industrial pollutants) to coastal water [e.g., *Brovelli et al.*, 2007; *Burnett et al.*, 2003; *Johannes*, 1980]. Chemical loading rates via SGD are strongly controlled by
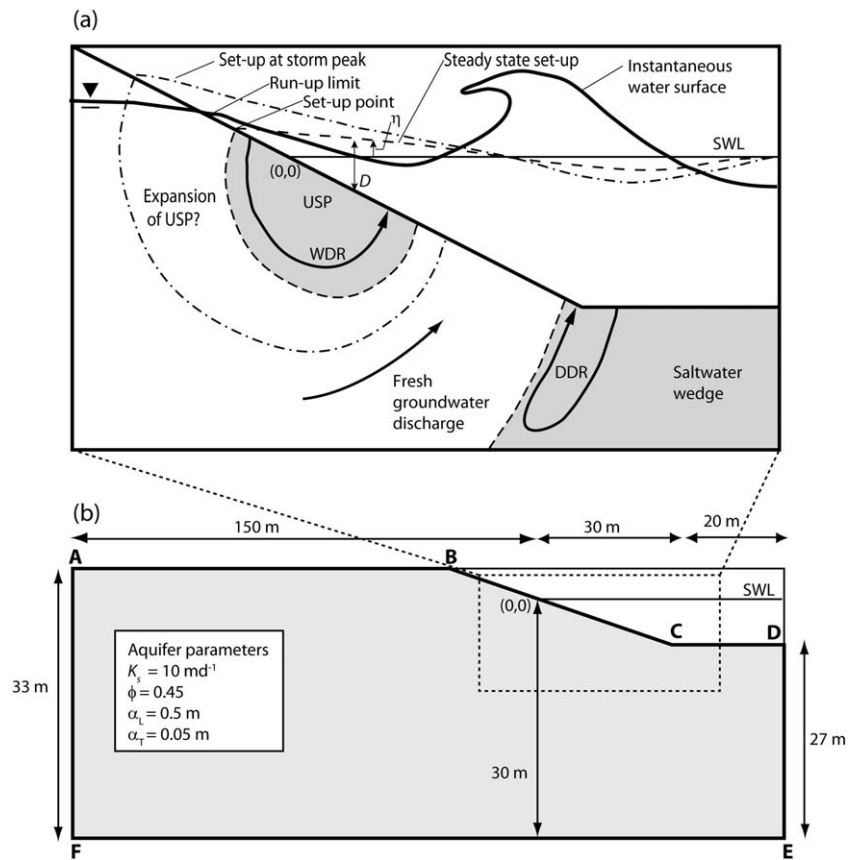
[1]Department of Civil and Environmental Engineering, Western University, London, Ontario, Canada.
[2]National Centre for Groundwater Research and Training, School of Civil Engineering, University of Queensland, Brisbane, Queensland, Australia.
[3]State Key Laboratory of Hydrology-Water Resources and Hydraulic Engineering, Hohai University, Nanjing, China.
[4]Laboratoire de technologie écologique, Institut d'ingénierie de l'environnement, Faculté de l'environnement naturel, architectural et construit, Ecole Polytechnique Fédérale de Lausanne, Lausanne, Switzerland.

Corresponding author: C. Robinson, Department of Civil and Environmental Engineering, Western University, London, ON N6A 5B9, Canada. (crobinson@eng.uwo.ca)

the subsurface flow paths and geochemical conditions in the aquifer, particularly near the shore [*Kroeger and Charette*, 2008; *Robinson et al.*, 2009; *Slomp and van Cappellen*, 2004; *Spiteri et al.*, 2008a; *Westbrook et al.*, 2005]. Due to the different chemical compositions of meteoric groundwater and seawater, the mixing of these waters as seawater recirculates through the nearshore aquifer can create an important reaction zone [*Appelo*, 1994]. This zone, termed a subterranean estuary [*Moore*, 1999], is typically characterized by strong geochemical gradients (e.g., pH and redox) where land-derived chemicals may be transformed or attenuated prior to their discharge [*Charette et al.*, 2005; *Hays and Ullman*, 2007; *Loveless and Oldham*, 2010; *Spiteri et al.*, 2005]. This zone also plays an important role in the transformation of sea-derived constituents recirculating through the nearshore aquifer [*Anschutz et al.*, 2009; *Spiteri et al.*, 2008b].

[3] Driven by density gradients, seawater intrudes the aquifer forming a saltwater wedge [*Diersch and Kolditz*, 2002; *Smith*, 2004; *Voss and Souza*, 1987; *Werner et al.*, 2013]. In the absence of sea level oscillations, the dispersion (mixing) zone along the saltwater wedge interface is the primary area of salt-freshwater mixing in a nearshore aquifer [*Moore*, 1999]. However, sea level oscillations occur at natural coasts due to tides and waves. Tides acting on a sloping beach face drive water exchange across the

Figure 1. (a) Conceptual diagram of the water levels, groundwater flows, and salinity distribution in a nearshore aquifer exposed to waves. The still water level (SWL), instantaneous water surface (thick solid line), and wave setup profiles (phase-averaged water surface) for the steady-state condition (prestorm and poststorm, dashed line) and storm peak (dash-dotted line) are shown. The upper saline plume (USP) formed by wave-driven recirculation (WDR) is shown in addition to the potential expansion of the USP in response to the storm. The saltwater wedge formed by density-driven recirculation (DDR) is also shown. (b) Numerical model domain and parameters. The dashed box in Figure 1b illustrates the nearshore zone highlighted in Figure 1a.

aquifer-ocean interface with infiltration dominating in the upper intertidal region and exfiltration dominating near the low-tide mark. This can result in the formation of an upper saline plume (USP) in addition to the saltwater wedge [*Boufadel*, 2000; *Mango et al.*, 2004; *Robinson et al.*, 2007b]. In the presence of waves, a USP may also form because waves induce an onshore upward tilt in the phase-averaged sea level (wave setup; Figure 1a). This pressure gradient sets up a seawater recirculation cell through the nearshore aquifer that extends from the maximum wave runup to wave-breaking point [*Bakhtyar et al.*, 2012, 2013; *Li and Barry*, 2000; *Longuet-Higgins*, 1983; *Xin et al.*, 2010]. Recently, *Xin et al.* [2010] simulated the combined effects of both tides (semidiurnal) and constant swell waves acting on a sloping beach and showed that when these forces are combined a more extensive USP is created with increased seawater recirculation across the aquifer-ocean interface. When a USP forms, the fresh groundwater discharge location is pushed seaward and is confined between the saltwater wedge and the USP (Figure 1a) [*Boufadel*, 2000; *Robinson et al.*, 2007b; *Xin et al.*, 2010]. Characterized by significantly faster seawater recirculation rates and

shorter transit times than the saltwater wedge [*Robinson et al.*, 2007b], the USP represents an active zone of salt-freshwater mixing in a nearshore aquifer.

[4] For regular oceanic forcing conditions (semidiurnal tides, constant swell waves), the salt-freshwater mixing in a subterranean estuary is driven primarily by hydrodynamic dispersion enhanced by flow oscillations and to a limited extent density instabilities (for USP). *Robinson et al.* [2007a] and *Abarca et al.* [2013] presented field and numerical results that demonstrated strong influences of spring-neap tidal variations on pore-water flow and solute (salt) transport in the nearshore aquifer. *Robinson et al.* [2007a] showed that the tidal variations caused significant changes in the salinity distribution with the USP contracting and expanding between the spring and neap tides (period = 14.78 days). At the field site of *Abarca et al.* [2013], due to the different magnitude of the new moon and full moon spring tides, the USP expanded and contracted at a period of 4 weeks. The extent of variation in the USP size observed by *Abarca et al.* [2013] was greater than reported by *Robinson et al.* [2007a]. For both studies, the oscillation of the USP driven by the longer period spring-neap tidal
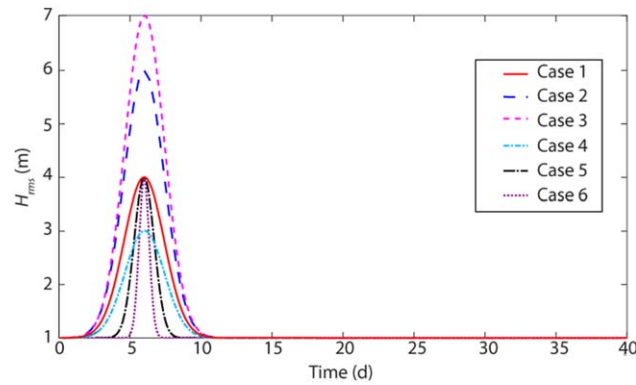
Figure 2. Synthetic wave events simulated. Cases 7–14 consider the same wave event as Case 1.

variations caused much greater salt-freshwater mixing than induced by the semidiurnal tidal fluctuations. Varying wave conditions may also modify significantly the nearshore aquifer dynamics, causing large displacement of the USP, especially for longer-duration events with large wave height variations. Therefore, wave events may have a significant impact on the salt-freshwater mixing and the geochemical conditions in a subterranean estuary.

[5] A number of investigations have examined coastal aquifer salinization caused by episodic (very large) storm events where the beach is overtopped and the coastal plain is inundated by seawater. These storm events can have a significant and long-lasting (order of months) influence on the salinity distribution and flows in a coastal aquifer. Effects of storms on a coastal aquifer system however are not limited to extreme events. Changes in subsurface flow patterns and salinity distributions are also induced by small offshore storms that generate intensified wave conditions along a shoreline. *Cartwright et al.* [2004] conducted a field study on a sandy beach aquifer and showed considerable oscillations of the saltwater wedge (3–5 m) in response to a wave event during which the significant wave height increased from 0.4 to 4.5 m over a period of ~2 days. *Li et al.* [2004] developed an analytical expression to describe

water table fluctuations induced by intensified wave conditions. While studies have revealed the influence of intensified wave conditions on the nearshore aquifer, the effect on the groundwater flows, solute transport, salt-freshwater mixing, and water exchange rates remain poorly quantified. Also, the time scales for the response to and recovery of the system from wave events are not clear. With smaller offshore storms occurring frequently and generating intensified wave conditions along coastlines [*Nielson*, 2009], this knowledge is needed to better understand salt-freshwater mixing dynamics and geochemical conditions in a nearshore aquifer.
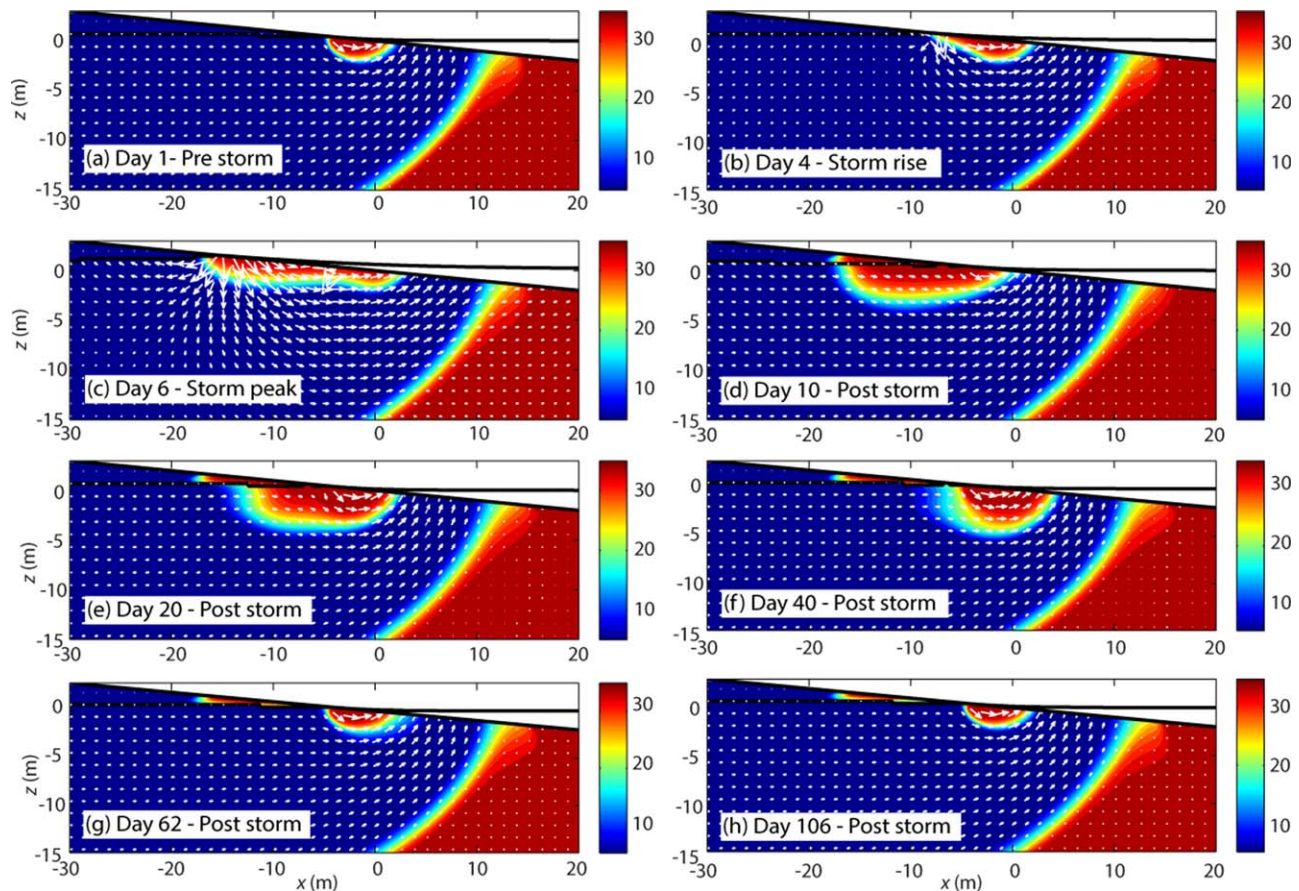
[6] In this study, numerical simulations were conducted to examine the impact of intensified wave conditions induced by an offshore storm on groundwater flow and salt transport in a nearshore aquifer. Simulated events with increased wave height (up to $H_{rms} = 7$ m) were considered: these provided the seaward boundary condition specified via time-varying wave-induced onshore hydraulic gradients (wave setup). Tidal fluctuations were not simulated, and as such the findings are pertinent for microtidal beaches that are dominated by wave rather than tidal effects [*Masselink and Short*, 1993]. Wave events will also impact the groundwater flows and salt transport in tidally influenced beaches, and the combined effects of tides and waves will lead to more complex conditions as suggested by *Xin et al.* [2010]. Large episodic events (e.g., hurricanes and tsunami) that result in beach overtopping and seawater inundation of the coastal plain are also beyond the scope of this study. The aim was to quantify the influence of a wave event on the water and salt exchange across the aquifer-ocean interface, groundwater flows, and salinity distribution in the aquifer. Key controlling variables including the intensity and duration of the wave event, the magnitude of fresh groundwater discharge, hydraulic conductivity, and beach slope were examined.

2. Numerical Model

[7] A numerical model based on SUTRA [*Voss and Provost*, 2002] was developed to simulate variably

Table 1. Simulated Cases With Model Parameter Values and Key Results

	Input Parameters					Salt Mass in USP				Water Influx/Efflux		
Case	H_{rms}^{INC} (m)	F (d)	Q_f (m³ d⁻¹)	K (m d⁻¹)	β	Change in Salt Mass (kg m⁻¹)	Maximum Salt Mass (kg m⁻¹)	5% Recovery Time (days)	10% Recovery Time (days)	Total Storm-Driven Influx (m³ d⁻¹ m⁻¹)	Maximum Influx (m³ d⁻¹ m⁻¹)	Maximum Efflux (m³ d⁻¹ m⁻¹)
1	3	2	2.1	10	0.1	369	471	79	62	20.2	7.6	5.8
2	5	2	2.1	10	0.1	623	726	134	99	33.9	13.3	7.5
3	6	2	2.1	10	0.1	758	861		115	53.8	17.3	8.2
4	2	2	2.1	10	0.1	241	344	59	49	16.6	5.8	5.0
5	3	1	2.1	10	0.1	216	319		154	11.1	8.7	5.5
6	3	0.5	2.1	10	0.1	127	230		78	6.0	10.5	5.2
7	3	2	3.15	10	0.1	325	375	55	46	18.1	7.3	6.4
8	3	2	1.4	10	0.1	430	613	124	88	22.3	8.2	5.5
9	3	2	1	10	0.1	477	752		96	23.2	8.3	5.2
10	3	2	2.1	50	0.1	2412	3101	52	48	54.1	37.7	30.4
11	3	2	2.1	21	0.1	749	1030	63	51	39.7	16.7	12.1
12	3	2	2.1	6.66	0.1	282	233	83	70	12.2	5.7	4.1
13	3	2	2.1	10	0.075	379	486	104	86	23.8	8.1	5.4
14	3	2	2.1	10	0.05	351	449		126	22.2	7.8	4.6

Figure 3. Instantaneous salt concentration (color bars are salinity in ppt) and flow velocities (vectors) for Case 1. The elapsed times are given in the figure legends. The black lines indicate the wave setup, water table elevation, and the aquifer-ocean interface. The results for days 62 and 106 are provided as these correspond to the times when the mass of salt in the upper aquifer domain had recovered to within 10% and 1% (surplus), respectively, of the prestorm condition.

saturated, density-dependent pore-water flow and salt transport in an unconfined coastal aquifer subject to time-varying wave forcing conditions (Figure 1). This model is similar to that used and described by *Xin et al.* [2010].

[8] The model domain represented a 2-D cross-shore transect through a homogeneous and isotropic coastal aquifer with a thickness of 33 m and a sloping beach boundary (beach slope = 0.1; Figure 1b). It was assumed that groundwater flow and solute transport were negligible in the alongshore direction. The *x-z* coordinate origin was located at the shoreline location corresponding to the still sea water level. With the exception of the wave forcing conditions, the parameters and boundary conditions adopted for the base case (Case 1) were the same as for the base case of *Xin et al.* [2010]. The parameter values were representative of a typical sandy coastal aquifer system [*Robinson et al.*, 2006] with hydraulic conductivity $K_s = 10$ m d^{-1}, porosity $\phi = 0.45$, longitudinal dispersivity $\alpha_L = 0.5$ m, and transverse dispersivity $\alpha_T = 0.05$ m. For the *van Genuchten* [1980] formulas, $S_{Wres} = 0.1$ while the parameters n and α were set to 14.5 m^{-1} and 2.68, respectively [*Carsel and Parrish*, 1988].

[9] *Xin et al.* [2010] recently demonstrated that a wave setup approach can be adopted to simulate the effects of

waves acting on the seaward boundary rather than simulating instantaneous waves. This approach is significantly more efficient and retains the key effects of waves on the groundwater flow and solute transport processes as well as the exchange of water and solutes across the aquifer-ocean interface. Using an empirical formula of *Nielson* [2009], we determined the mean sea surface elevation (averaged over a wave period), η (m):

$$\eta = \frac{0.4 H_{rms}}{1 + 10 \frac{D + \eta}{H_{rms}}} \quad (1)$$

where H_{rms} (m) is the root-mean-square wave height at time t and D (m) is the still water depth at location x (Figure 1a). This expression was solved for η, which thereby defined the hydraulic head condition on the seaward boundary of the groundwater model. Other solutions describing wave setup are available, including that by *Longuet-Higgins* [1983], or alternatively, as done by *Xin et al.* [2010], the instantaneous wave motion predicted by a shallow water wave simulator such as BEACHWIN [*Li et al.*, 2002] may be used to derive the mean sea surface elevation with the wave setup effect included. Equation (1) does not consider wave runup (in the swash zone further inland) and

may thus predict a smaller wave setup compared with those of *Longuet-Higgins* [1983] and *Li et al.* [2002]. As this study focused on providing mechanistic insights into the effects of a wave event on nearshore aquifer dynamics and the time scale of the system's response, the numerical findings are expected to be consistent regardless of the specific solution adopted to simulate wave setup.

[10] Synthetic time series of H_{rms} were generated to represent a wave event of a given duration and intensity (Figure 2) using:

$$H_{rms}(t) = H_{rms}^{ss} + H_{rms}^{INC} \exp\left[-\left(\frac{t - T_{max}}{F} \right)^2 \right], \qquad (2)$$

where T_{max} [T] is the time at which the maximum wave height occurs (day 6 for all simulations); F [T] is a parameter that controls the duration of the wave event (period of the wave event is equal to approximately $5F$); H_{rms}^{ss} is the steady-state wave height (prewave and postwave event); and H_{rms}^{INC} is the maximum increase in wave height. Synthetic wave events were simulated so that the response and recovery of the nearshore aquifer could be readily quantified. Note that equation (2) has been found to describe well the wave height variations over real offshore storm events [*Cartwright et al.*, 2004].

[11] For all simulations performed, H_{rms}^{ss} was set to 1 m. Cases were simulated with F varying from 0.5 to 2 days and H_{rms}^{INC} varying from 2 to 6 m (Table 1). Along a typical wave-exposed coastline, the smaller wave events simulated (i.e., $H_{rms}^{INC} = 2$) would occur relatively often (order of months), whereas the large wave events simulated would be infrequent (order of decades). To put into context, historical data for the New South Wales (Australia) coastline with a moderate wave climate show that the maximum wave heights (H_{rms}) for return periods of 0.1, 1, 10, and 50 years are 2.5, 3.8, 4.9, and 5.7 m, respectively [*Shand et al.*, 2010].

[12] Additional simulations were conducted to examine the extent to which land-derived groundwater flux, the aquifer permeability, and the beach slope altered the system's response to the intensified wave conditions (Table 1). Aquifer hydraulic conductivities ranging from $K = 6.66$ to 50 m d^{-1} were considered. This range represents the permeability of medium sand which is common on wave-dominated beaches. Although K can vary over several orders of magnitude in nearshore aquifers, the K range considered was constrained by the model domain adopted. For example, higher K values reduced the landward hydraulic gradient, and subsequently, the intrusion of the saltwater wedge became restricted by the landward model boundary. Beach slopes from steep ($\beta = 0.1$) to moderately steep ($\beta = 0.05$) were examined. The range of β considered was restricted by the wave setup formula used (equation (1)) which is not applicable for more mildly sloping beaches ($\beta < 0.05$).

[13] The boundary condition applied on the aquifer-ocean interface (BCD) depended on the sea surface elevation (η), which varied with the wave height (Figure 1). The submerged nodes along the interface (below the sea surface) were prescribed by the hydrostatic pressure corresponding to the local mean water depth described by (1).
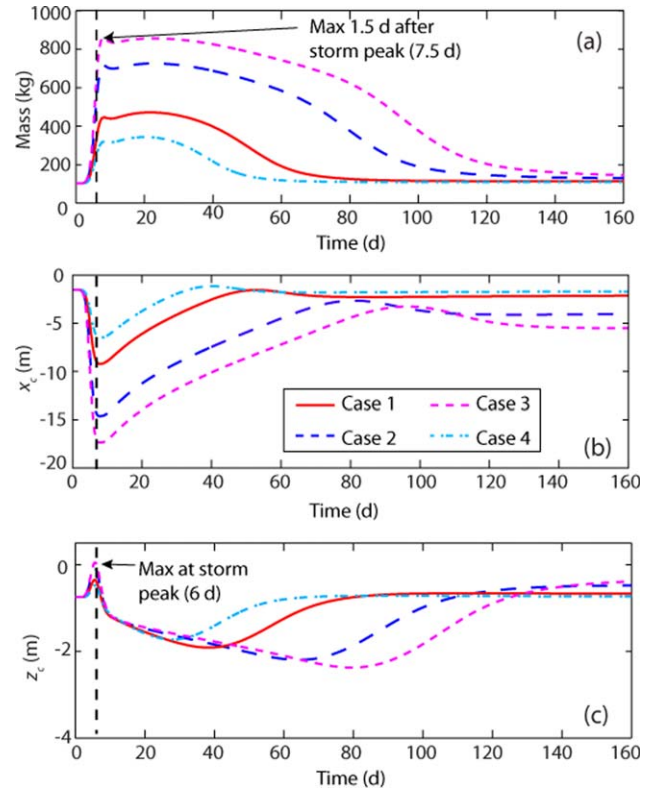
Figure 4. (a) Total salt mass per unit width of aquifer in the USP, (b) x coordinate of centroid (x_c), and (c) z coordinate of centroid (z_c) of salt in the USP for Case 1 ($H_{rms}^{INC} = 3$ m), Case 2 ($H_{rms}^{INC} = 5$ m), Case 3 ($H_{rms}^{INC} = 6$ m), and Case 4 ($H_{rms}^{INC} = 2$ m). The time of the storm peak (6 days) is indicated by the vertical black dashed line.

Above the sea surface the exposed nodes were either (a) considered seepage face nodes with local pressure equal to the atmospheric pressure ($P = 0$) if the nodes were saturated at the previous time step or (b) treated as part of the no-flow boundary above the seepage face if the nodes were unsaturated at the previous time step. The maximum wave setup point never exceeded the apex of the sloped beach face (B). Influx to the aquifer across the interface had a salt concentration of 35 ppt (mass fraction) and at nodes with efflux (from the aquifer), a zero concentration gradient was specified. The vertical seaward boundary condition (DE) was no flow. The location of this boundary was set sufficiently far from the shoreline (at $x = 50$ m) so as not to influence the nearshore subsurface flow and transport.

[14] A uniform, constant flux (Q_f) was specified along the vertical landward boundary (AF) to simulate fresh groundwater flow toward the sea. For all simulations except Cases 7–9, the flow rate through the landward boundary was specified as 2.1 m^3 d^{-1} m^{-1} width of aquifer with a background salt concentration of 1 ppt. This Q_f corresponds with the estimated freshwater flux at a field site on Moreton Island, Australia [*Robinson et al.*, 2006]. The bottom model boundary (EF) was an impermeable aquifer base and thus set as a no-flow boundary. The upper boundary (AB) was also a no-flow boundary with rainfall and evaporation neglected.
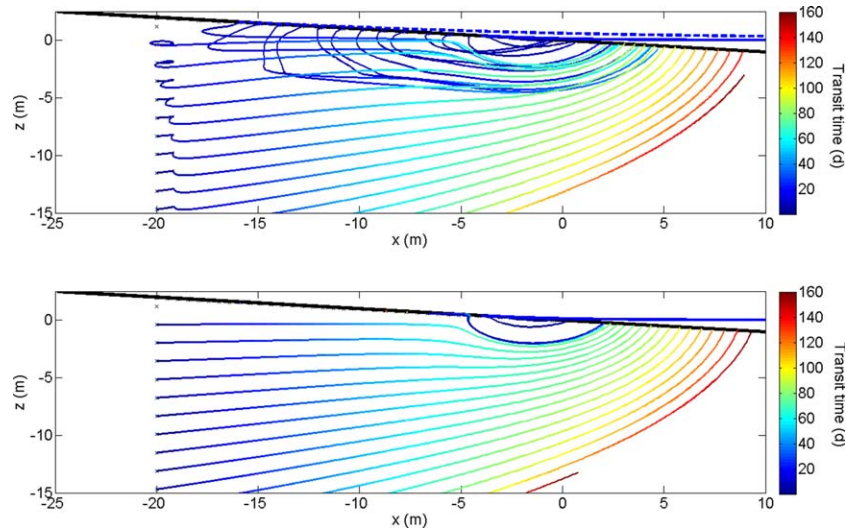
Figure 5. Simulated flow paths for saltwater particles and freshwater particles transported through the nearshore aquifer for (a) Case 1 and (b) steady-state conditions with $H_{rms} = 1$ m. Transit times along each flow path are depicted by the colored line shading. Note that in Figure 5a the freshwater and saltwater particle flow lines cross in space but not in time. Under the steady-state condition, there was only a narrow wave-induced seawater infiltration zone from $x = -5$ to -2.5 m, and infiltrating saltwater particles had considerably shorter transit times. The blue dashed line above the aquifer-ocean interface (black solid line) in Figure 5a depicts the mean sea water level at the peak of the wave event ($H_{rms} = 4$ m), and the blue solid line in Figures 5a and 5b depicts the steady-state mean sea water level ($H_{rms} = 1$).

[15] The model was initially run to steady state with the prestorm wave condition ($H_{rms}^{ss} = 1$ m) applied at the seaward boundary. The model was then run with a time-varying seaward boundary condition to simulate the wave events shown in Figure 2. Each time-varying simulation was run for a total simulation time of 160 days. This time was required for the aquifer to return to prestorm conditions. The initial steady-state model was the same for Cases 1–6, but different for the remaining cases due to the changes in Q_f, β, and K. The initial steady-state flows and salt concentrations for Cases 1–6 can be seen in Figure 3a. Further details of the model including the model setup and grid discretization are given by *Xin et al.* [2010].

3. Results and Discussion

3.1. Effect of Intensified Wave Conditions (Case 1)

[16] The simulated salinity distribution and flow velocity vectors in the nearshore aquifer before, during, and after the wave event for Case 1 are shown in Figure 3. As expected, the groundwater flows and salinity distribution in the aquifer were significantly modified by the intensified wave conditions. At the initial steady state, the onshore pressure gradient corresponding to $H_{rms} = 1$ m led to a seawater recirculation cell through the shallow aquifer. This formed a USP that extended up to the wave setup point ($x \approx -5$ m, Figure 3a). As previously shown by *Xin et al.* [2010], the wave-induced recirculations push fresh groundwater to discharge seaward of the USP. The flow pattern and salinity distribution were similar to those observed in aquifers subjected to simple harmonic tidal fluctuations (e.g., semidiurnal) [*Boufadel*, 2000; *Mango et al.*, 2004;
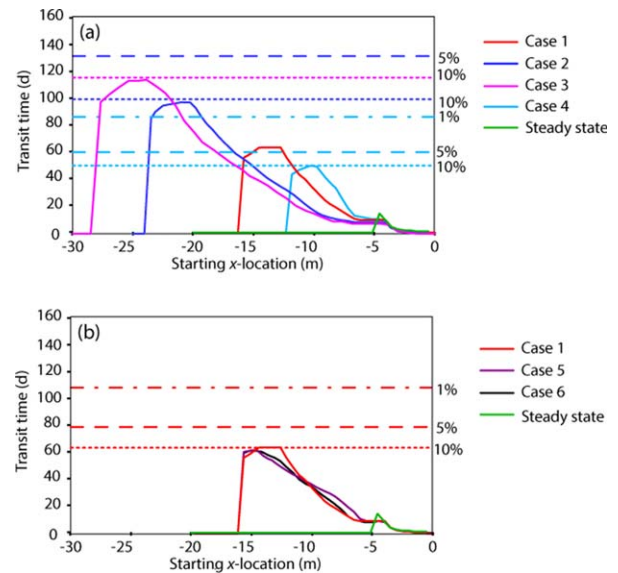

Figure 6. Transit times for seawater particles to recirculate through the aquifer as a function of their starting x location along the aquifer-ocean interface for cases with varying (a) magnitude of the wave event (H_{rms}^{INC}) and (b) wave event duration (F). The horizontal lines denote the time calculated for the mass of salt in the USP to recover to within 10% (dashed line), 5% (dotted line), and 1% (dash-dotted line) of the prestorm condition. The recovery times for Cases 2, 3, and 4 are shown in Figure 6a, and recovery times for Case 1 (red lines) are shown in Figure 6b. The recovery times are not shown for Cases 5 and 6 as they are similar to that of Case 1. For Case 2 the mass in the USP does not return to within 1%, and for Case 3 it does not return to within 5% of the prestorm conditions over the 160 day simulation period.
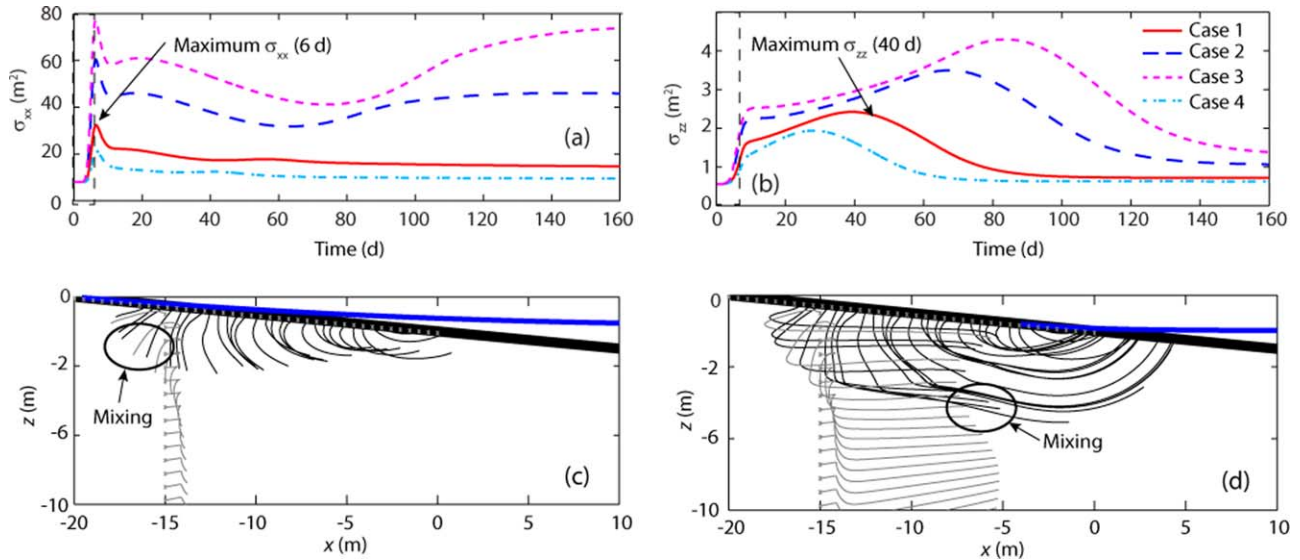
Figure 7. (a) Horizontal variance (σ_{xx}), and (b) vertical variance (σ_{zz}) of salt in the USP for Case 1 ($H_{rms}^{INC}=3$ m), Case 2 ($H_{rms}^{INC}=5$ m), Case 3 ($H_{rms}^{INC}=6$ m), and Case 4 ($H_{rms}^{INC}=2$ m). The particle tracking results at 6 days (maximum σ_{xx}) and 40 days (maximum σ_{zz}) for Case 1 are provided in Figures 7c and 7d, respectively. The black lines show the flow paths for saltwater particles originating along the aquifer-ocean interface, and the grey lines show the flow paths for freshwater particles originating at $x = -15$ m. The similar locations of the freshwater and saltwater particles indicate mixing of the two waters.

Mao et al., 2006; *Robinson et al.*, 2006, 2007b; *Xin et al.*, 2010].

[17] The recirculating flow strengthened and the USP expanded as the wave height increased (Figure 3b). The USP initially expanded horizontally as seawater moved landward and infiltrated the foreshore area in response to the increased wave setup. The USP reached its maximum horizontal extent at the peak of the wave event (Figure 3c): at this time the wave setup point was at its most landward position. As the wave height decreased, the USP gradually contracted horizontally, but with seawater continuing to infiltrate on the upper part of the beach, the USP expanded in the vertical direction (Figure 3d). Once infiltrated, seawater moved downward along a discharge flow path to the sea (Figures 3e and 3f). The observed extent of expansion and contraction of the USP over the wave event was similar to that observed by *Abarca et al.* [2013] in response to spring-neap tidal variations. However, unlike the cyclic variations induced by spring-neap variations, wave-induced changes to the USP are driven by an irregular forcing, and in some cases there may be a lengthy time gap between successive wave events. For the conditions simulated there was a significant time delay before the salinity distribution in the nearshore aquifer returned to prestorm conditions (Figures 3g and 3h). Further, it is evident that residual salt was trapped in the unsaturated zone beneath the beach face as the wave event passed (Figures 3d–3h). This was due to the rapid fall of the water table as the wave height decreased, leaving the salt behind in an unsaturated zone with relatively weak flow and solute transport. A similar salt trapping effect was observed by *Lenkopane et al.* [2009] in numerical simulations of a riparian zone exposed to tidal and seasonal estuarine salinity and water level fluctuations. In reality the trapped salt
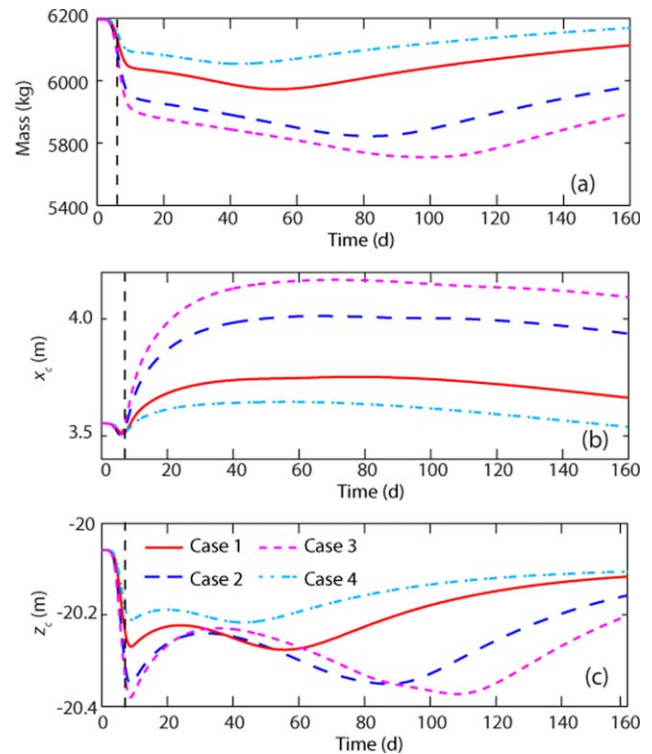
Figure 8. (a) Total salt mass per unit width of aquifer in the saltwater wedge, and (b) x coordinate of centroid (x_c) and (c) z coordinate of centroid (z_c) of the saltwater wedge for Case 1 ($H_{rms}^{INC}=3$ m), Case 2 ($H_{rms}^{INC}=5$ m), Case 3 ($H_{rms}^{INC}=6$ m), and Case 4 ($H_{rms}^{INC}=2$ m). The time of the peak of the (6 days) is indicated by the vertical black dashed line.
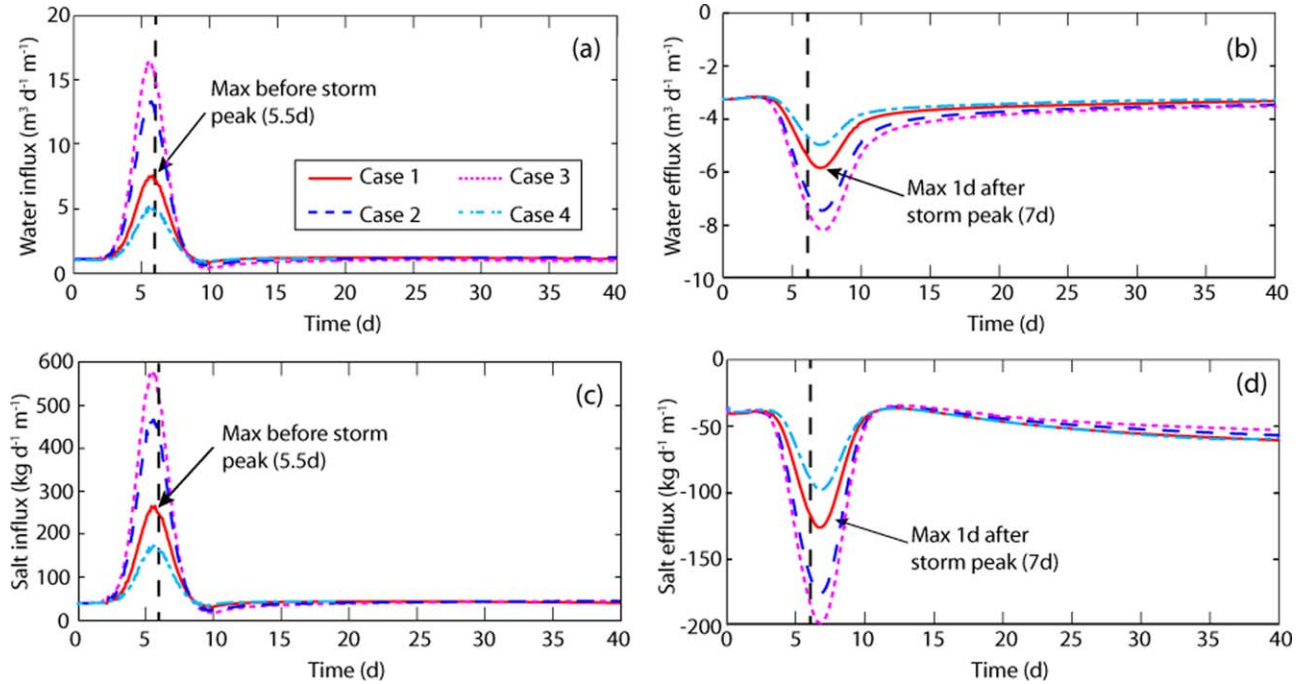
Figure 9. (a) Water influx, (b) water efflux, (c) salt influx, and (d) salt efflux across the aquifer-ocean interface for Case 1 ($H_{rms}^{INC}=3$ m), Case 2 ($H_{rms}^{INC}=5$ m), Case 3 ($H_{rms}^{INC}=6$ m), and Case 4 ($H_{rms}^{INC}=2$ m). The time of the storm peak (6 days) is indicated by the vertical black dashed line.

may be flushed through the shallow beach sediments by rainfall. This was not considered in the simulations. Spatial moments of salt concentrations were calculated to quantify the response of the salinity distribution to the wave event (see supporting information for calculation details). Spatial moments were calculated separately for the USP and salt-water wedge to analyze their individual behavior. This was done by dividing the model domain into two separate integration domains (upper and lower) by locating the minimum concentrations separating these two saline plumes. The background salt concentration (1 ppt) was subtracted from the salt concentrations before the moments were calculated so that only salt originating from the seawater was considered in the calculation. From Figure 4a it can be seen that the salt mass in the USP increased rapidly in response to the increase in wave height. The maximum salt mass in the aquifer occurred 1.5 days after the peak of the wave event (at 7.5 days) with salt continuing to infiltrate the foreshore more rapidly than it could exfiltrate further offshore. As the waves receded the salt mass decreased gradually with the USP slowly returning to the prestorm condition. The salt mass in the USP returned to within 10%, 5%, and 1% (surplus) of its initial (prestorm) mass at 62, 79, and 106 days, respectively. Consistent with the evolution of salt distribution shown in Figure 3, the centroid of the plume moved rapidly landward and upward in response to the intensified waves as seawater infiltrated further landward (Figures 4b and 4c). After the storm peak, the centroid of the plume moved downward and gradually seaward.

[18] Particle tracking was performed to examine the advective flow paths and corresponding transit times for seawater recirculating and fresh groundwater discharging through the aquifer. Particle tracking was conducted in MATLAB using the element centroid velocities output by SUTRA. Particles were released along a vertical line at $x = -20$ m with 1 m vertical interval (called freshwater particles) and along the aquifer-ocean interface at 0.5 m interval (called saltwater particles). The particle tracking started at the beginning of the simulation. The particle flow paths including transit times for Case 1 are shown in Figure 5a. For comparison, the particle tracking results for steady-state conditions ($H_{rms} = 1$ m) are also provided (Figure 5b). The intensified wave conditions significantly altered the transport pathways of the saltwater particles. The particles that infiltrated near the maximum wave setup point ($x = -17$ to -15 m) had a shallower pathway than those that infiltrated seaward of this point ($x = -14$ to -12 m). This is because the latter particles were exposed to downward flow induced by the wave setup for a longer period of time than the former particles, which were subjected to this condition only at the peak of the storm. During the wave event the saltwater particles moved downward and crossed into the prestorm flow paths of freshwater particles. As the wave event passed the saltwater particles then discharged along the freshwater path lines. Note that the overlap between the saltwater and freshwater flow paths occurs only spatially with the particles not crossing the same locations at identical times. The successive spatial overlap between the paths of saltwater and freshwater particles is consistent with aquifer salinization and freshening as the USP expanded and contracted.

[19] The transit times for the saltwater particles to travel through the aquifer as a function of their starting x coordinate along the aquifer-ocean interface are shown in Figure 6. For Case 1 the transit times were longest for particles
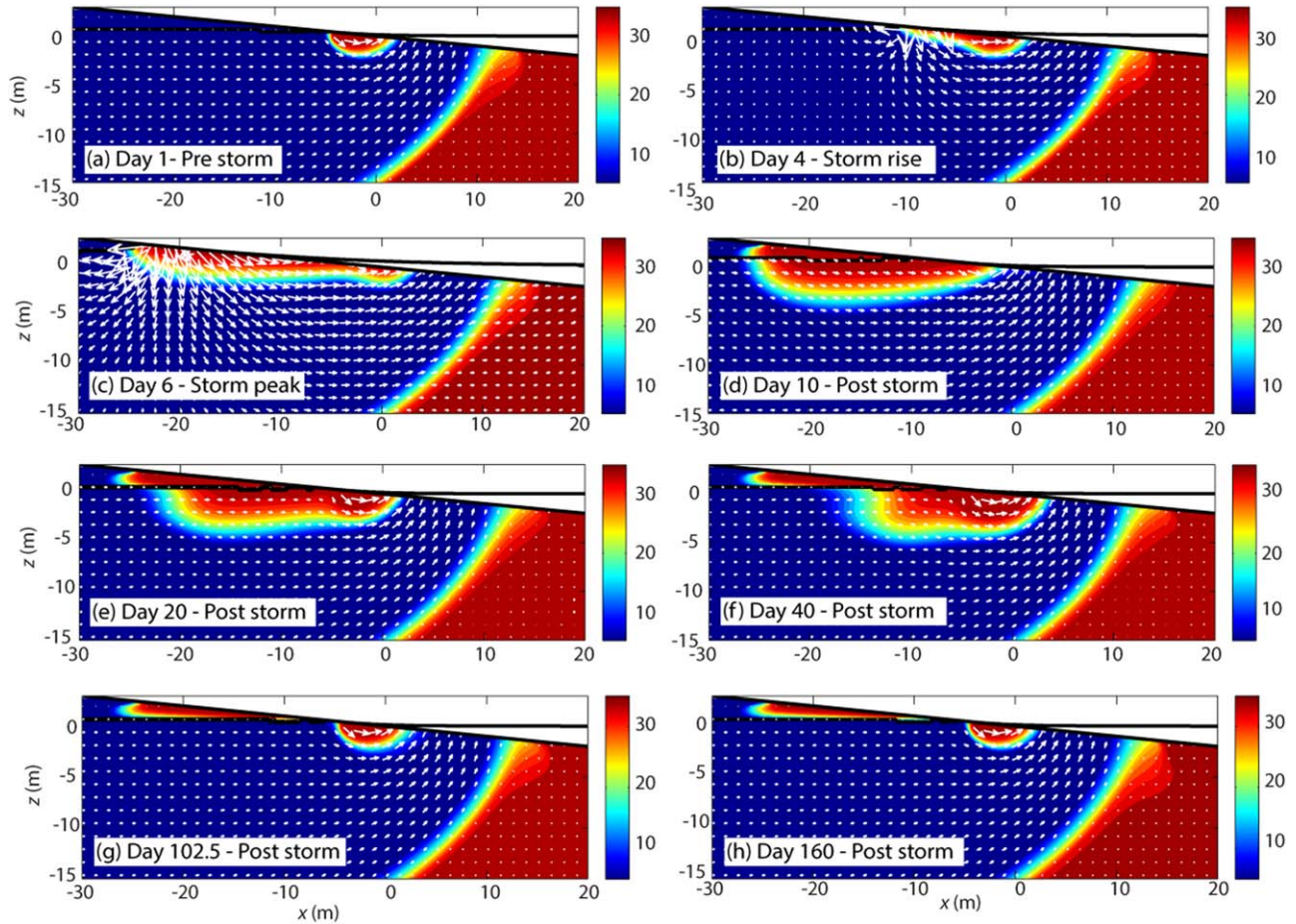
Figure 10. Instantaneous salt concentration (color bars are salinity in ppt) and flow velocities (vectors) for Case 2. The elapsed times are given in the figure legends. The black lines indicate the wave setup and water table elevation. The result for day 102.5 corresponds to the time when the mass of salt in the upper aquifer had recovered to within 10% (surplus) of the prestorm condition. At the end of the simulation (160 days) the mass of salt in the upper aquifer had recovered to within 2.5% (surplus) of the prestorm condition.

infiltrating just seaward of the maximum wave setup point, between $x = -14$ and -12 m. This was consistent with the longer and deeper flow paths of these particles (Figure 5a). The transit times were slightly less for particles infiltrating close to the maximum wave setup point (between $x = -14$ to -16 m) due to their shallower and shorter flow paths. The

transit times decreased almost linearly seaward of $x = -12$ m as the flow path lengths decreased toward the center of the flow recirculation cell. The time for the total salt mass in the upper aquifer domain (USP) to recover to within 10%, 5%, and 1% (surplus) of the prestorm salt mass is presented in Figure 6b (red horizontal lines). The maximum saltwater
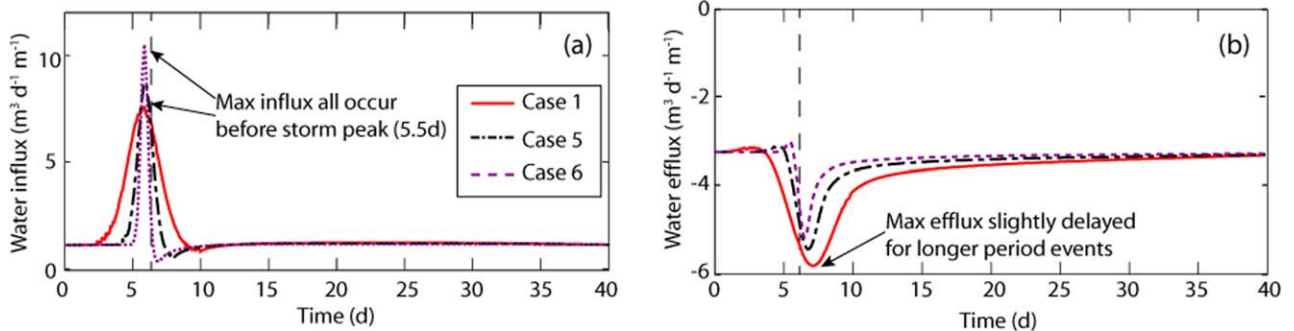
Figure 11. (a) Water influx and (b) water efflux for Case 1 ($F = 2$), Case 5 ($F = 1$), and Case 6 ($F = 0.5$). The time of the storm peak (6 days) is indicated by the vertical black dashed line.
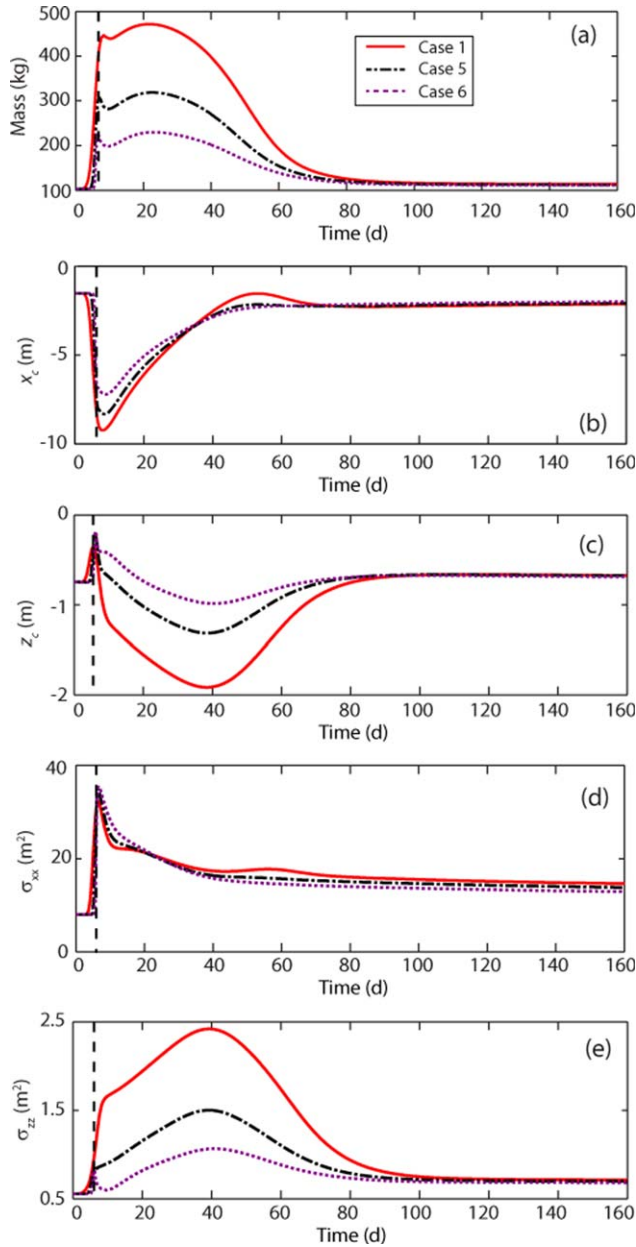
Figure 12. (a) Total salt mass per unit width of aquifer in USP and (b) x coordinate of centroid (x_c), (c) z coordinate of centroid (z_c), (d) horizontal variance (σ_{xx}), and (e) vertical variance (σ_{zz}) of salt in the USP for Case 1 ($F = 2$), Case 5 ($F = 1$), and Case 6 ($F = 0.5$). The time of the storm peak (6 days) is indicated by the vertical black dashed line.

particle transit times appear to be strongly related to the 10% (surplus) recovery time. This indicates that the long recovery of the salinity distribution in the upper aquifer was largely controlled by the advective transport of the infiltrated seawater. This result also demonstrates the importance of dispersive transport with approximately 10% of the excess salt remaining in the aquifer longer than the maximum advective transit time for saltwater particles (64 days). The importance of dispersive transport is reflected in the long 5% (79 days) and 1% (106 days; surplus) recovery times; the associated

salt-freshwater mixing is expected to lead to modifications in the geochemical conditions in a subterranean estuary.

[20] The wave event had much less impact on the fresh groundwater discharge flow paths. The transit times for the freshwater particles (released at $x = -20$ m) increased with aquifer depth due to the longer discharge flow path ($\sim$150 and $\sim$80 days for particles released at $z = -29$ m and $z = 0$ m, respectively; Figure 5). Other than the intensified wave conditions inducing a small localized circulation for freshwater particles in the upper aquifer, the event did not significantly alter the fresh groundwater pathways or transit times.

[21] The calculated variances of salt in the USP (Figures 7a and 7b) were consistent with salinity distributions (Figure 3) and the saltwater particle tracking results (Figure 5). The equations used to calculate the variance are provided in the supporting information. Both the horizontal and vertical variance increased sharply in response to the wave event. The horizontal spread was greatest at the peak of the wave event (6 days), consistent with the rapid seawater infiltration into the upper freshwater zone. The locations of freshwater and saltwater particles at 6 days are shown in Figure 7c. The similar locations for particles near the maximum wave setup point indicate that enhanced salt-freshwater mixing occurred at this location around the peak of the wave event (6 days). It should be noted that although the saltwater and freshwater particle locations are not exactly the same at a given time, hydrodynamic dispersion would cause mixing due to the close proximity of the particles. As the wave height decreased, the horizontal variance decreased as the USP contracted horizontally. In contrast, the vertical variance of the USP continued to increase for some time after the peak of the wave event. This is consistent with the downward movement of the saltwater that infiltrated just seaward of the maximum wave setup point into the freshwater zone. The maximum vertical variance occurred at $\sim$40 days. As seen in Figure 7d the large variance was associated with the enhanced fresh-saltwater mixing (similar locations for freshwater and saltwater particles) along the lower boundary of the USP. The variances slowly decreased to their prestorm values as the excess salt discharged from the aquifer.

[22] Although movement of the saltwater wedge interface was not clearly evident from the salt distributions (Figure 3), spatial moments reveal that the intensified wave conditions caused the total salt mass in the lower aquifer to decrease (Figure 8a). There was an abrupt decline in the salt mass in response to the storm event followed by a more gradual decrease in mass. This was likely due to the storm-induced horizontal and subsequent vertical expansion of the USP. As demonstrated by *Kuan et al.* [2012], the expansion of the upper seawater recirculation cell and thus the USP cause the saltwater wedge to retreat seaward. Consistent with the reduction in salt mass, the centroid (x, z) of the saltwater wedge shifted slightly seaward (Figures 8b and 8c). This shift was relatively small (by $\sim$0.15 m horizontally) due to the large salt mass associated with the saltwater wedge.

[23] In contrast to the salt distribution, the groundwater flows responded and recovered much faster to the changing wave conditions. This is evident from the total water exchange rates (influx and efflux) across the aquifer-ocean interface through the simulation period (Figure 9). For Case
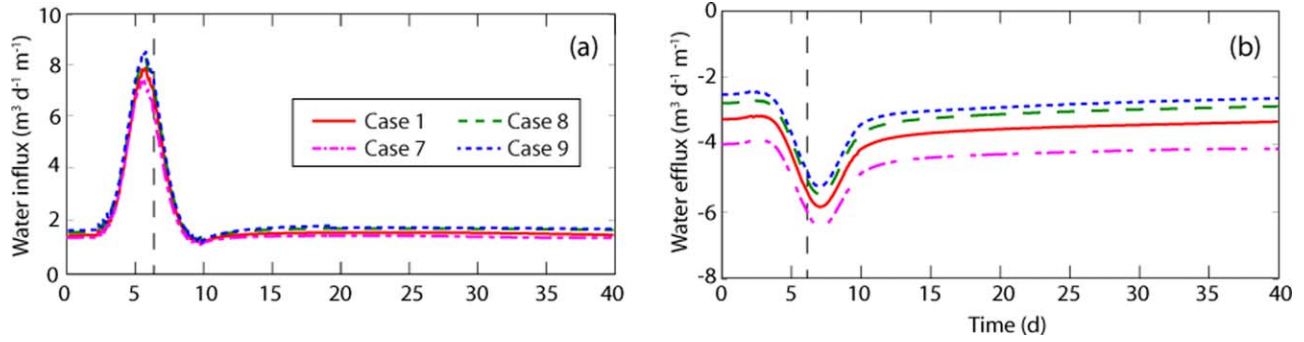
Figure 13. (a) Water influx and (b) water efflux for Case 1 (Q_f = 2.1 m^3 d^{-1}), Case 7 (Q_f = 3.15 m^3 d^{-1}), Case 8 (Q_f = 1.4 m^3 d^{-1}), and Case 9 (Q_f = 1 m^3 d^{-1}). The time of the storm peak (6 days) is indicated by the vertical black line.

1, it can be seen that (sea) water influx increased as the onshore pressure gradient strengthened. The maximum influx occurred 0.5 days before the storm peak with the highest influx rate occurring near the wave setup point at this time (Figure 9a). The influx was greatest at this time as the rate of change in the wave height, and therefore onshore movement of the wave setup point, was high combined with the strengthened offshore pressure gradient driving increased recirculation. The efflux was delayed slightly (maximum ∼1 day after the peak) and slightly more spread out relative to the influx (Figure 9b). The difference between the influx and efflux reflects the fact that the aquifer could fill more quickly than it could drain. The water exchange rates returned to within 1% of the prestorm rates within ∼10 days of the storm peak, i.e., at ∼16 days; this time lag was small compared with the response of the salt distribution. The maximum efflux (5.8 m^3 d^{-1} m^{-1}) was significantly greater than that predicted to be induced by regular wave forcing (3.3 m^3 d^{-1} m^{-1} for H_{rms} = 1 m (steady-state condition)) or semidiurnal tidal fluctuations (2.8 m^3 d^{-1} m^{-1} for tidal amplitude = 1 m) [*Robinson et al.*, 2007b] for the same aquifer conditions. It was also greater than that simulated by *Abarca et al.* [2013] to be induced by spring-neap tidal variations. For their case, a maximum efflux of ∼1.3 m^3 d^{-1} m^{-1} occurred around the highest spring tides.

[24] The response of the salt fluxes to the wave event was similar to that of the water fluxes (Figures 9c and 9d). The net salt flux was positive around the peak of the wave event corresponding to the increasing salt mass in the USP (Figure 4a). The maximum salt mass in the USP occurred at 7.5 days, which corresponds to the net salt flux (influx − efflux) becoming negative. For a long time after the storm (e.g., at 40 days), the net salt flux remained slightly negative as excess salt continued to discharge from the aquifer.

3.2. Effect of Magnitude of Wave Height Variation

[25] To examine the effect of the magnitude of the wave event on the nearshore aquifer dynamics simulations were conducted with H_{rms}^{INC} varying from 2 to 6 m (Cases 2–4, Figure 2). As expected the larger wave events increased the water and salt fluxes across the aquifer-ocean interface (Figure 9) and further modified the salinity distribution and groundwater flows. As shown in Figure 10 for Case 2 (H_{rms}^{INC} = 5 m), as the maximum wave setup point moved

further onshore with increased H_{rms}^{INC}, seawater infiltrated further landward and the initial horizontal and subsequent vertical expansion of the USP increased accordingly. Also, as the fall of the water table was more rapid with increased H_{rms}^{INC}, more residual salt was trapped in the unsaturated zone beneath the beach face as the wave event passed (Figure 10).

[26] The water and salt influx and efflux across the aquifer-ocean interface showed the same temporal response to the wave event for Cases 1–4, but the rates rose as the intensity of the wave event increased (Figure 9). For example, relative to Case 1 (7.6 m^3 d^{-1} m^{-1}; H_{rms}^{INC} = 3 m), the maximum instantaneous influx rose by 76% for Case 2 (13.3 m^3 d^{-1} m^{-1}; H_{rms}^{INC} = 5 m), 128% for Case 3 (17.3 m^3 d^{-1} m^{-1}; H_{rms}^{INC} = 6 m), and decreased by 25% for Case 4 (5.8 m^3 d^{-1} m^{-1}; H_{rms}^{INC} = 2 m). The total storm-driven influx was calculated for each case by integrating the increase in influx (influx above the steady-state influx rate) over the simulation period. As expected the total storm-driven influx also increased with the intensity of the wave event (53.8 m^3 m^{-1} for Case 3, cf. 20.2 m^3 m^{-1} for Case 1; Table 1). For all cases, the time of the maximum influx occurred 0.5 days prior to the peak of the wave event, and both the water and salt exchange rates returned rapidly to the prestorm conditions.

[27] Consistent with the salt distributions (Figures 3 and 10) and seawater influx rates, the increase in salt mass in the USP was greater for more intense wave events (Figure 4a and Table 1); so were the horizontal and vertical movement of the plume (Figures 4b and 4c) and the plume variance (Figures 7a and 7b). The temporal response of the spatial moments to the wave event was similar, i.e., a sharp increase in salt mass as the waves intensified followed by a period of relatively constant mass before the mass slowly decreased to the prestorm condition. Due to the larger disturbance, the time for the USP salt mass to return to the prestorm condition was greater for larger wave events (Case 3: 115 days, Case 2: 99 days, Case 1: 62 days, and Case 4: 49 days for the salt mass to return to within 10% of prestorm condition). It is evident from particle tracking results shown in Figure 6a that the longer recovery time of the salt distribution for the simulations with larger H_{rms}^{INC} was largely due to and corresponded with the longer advective transit times of saltwater particles infiltrating just seaward of the maximum wave setup point. The saltwater particles infiltrating this zone were pushed deeper into the
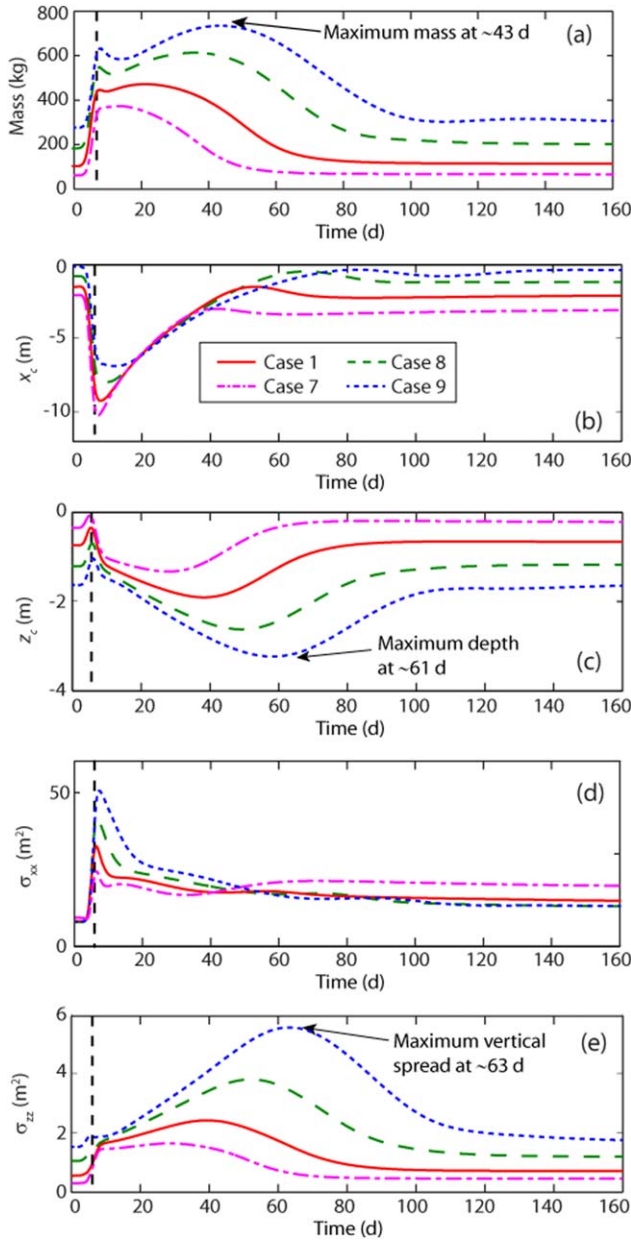
Figure 14. (a) Total salt mass per unit width of aquifer in USP and (b) x coordinate of centroid (x_c), (c) z coordinate of centroid (z_c), (d) horizontal variance (σ_{xx}), and (e) vertical variance (σ_{zz}) of salt in the USP for Case 1 ($Q_f = 2.1$ m^3 d^{-1}), Case 7 ($Q_f = 3.15$ m^3 d^{-1}), Case 8 ($Q_f = 1.4$ m^3 d^{-1}), and Case 9 ($Q_f = 1$ m^3 d^{-1}). The time of the storm peak (6 days) is indicated by the vertical black dashed line.

aquifer by the greater onshore pressure gradient, and so their flow pathway was lengthened. For Cases 2 and 3 the salt mass in the aquifer had not returned to prestorm conditions at the end of the simulation time, indicating the enhanced dispersion in the upper aquifer. The temporal variability in the spatial moments calculated for the saltwater wedge was similar for all cases with varying H_{rms}^{INC} but intensified wave conditions pushed the saltwater wedge further seaward near the freshwater discharge zone due the

larger expansion of the USP. This is evident in Figure 10 and supported by the decrease in salt mass and z_c and increase in x_c for the saltwater wedge for Cases 2 and 3 (Figure 8).

### 3.3. Effect of Duration of Wave Event

[28] Case 5 ($F = 1$ day) and Case 6 ($F = 0.5$ days) were conducted to evaluate the effect of the duration of the wave event on the aquifer response. The water influx and efflux rates and the spatial moments of the USP are shown in Figures 11 and 12, respectively. For a longer-duration wave event, more time was available for seawater to infiltrate the foreshore landward of the steady-state wave setup point. For all cases (Cases 1, 5, and 6) the period of increased water influx corresponded closely with the duration of the wave event with negligible time delay (Figure 11a). The shorter duration events led to a higher instantaneous water influx; however, the total water influx over the wave event increased as the duration of the event lengthened (Table 1).

[29] The greater total water influx led to a larger USP as indicated by the total salt mass in the upper aquifer domain (Figure 12a and Table 1). The temporal trends in the spatial moments were similar among Cases 1, 5, and 6 but with different magnitudes. The duration of the storm had a greater effect on the vertical expansion (Figures 12c and 12e) of the USP than the horizontal expansion (Figures 12b and 12d). This is because for all cases the maximum wave height and thus the excursion of the wave setup point were the same. For the longer-duration event, saltwater particles infiltrating near the maximum wave setup point were exposed to the onshore pressure gradient for a longer time period, and so these particles were pushed deeper into the aquifer. This led to the formation of a deeper USP.

[30] The time for the salt distribution in the upper aquifer to recover to within 10% (surplus) of the prestorm conditions was similar among the three cases: 62 days for Case 1, 61 days for Case 5, and 60 days for Case 5 (Table 1). These recovery times increased slightly as the duration of
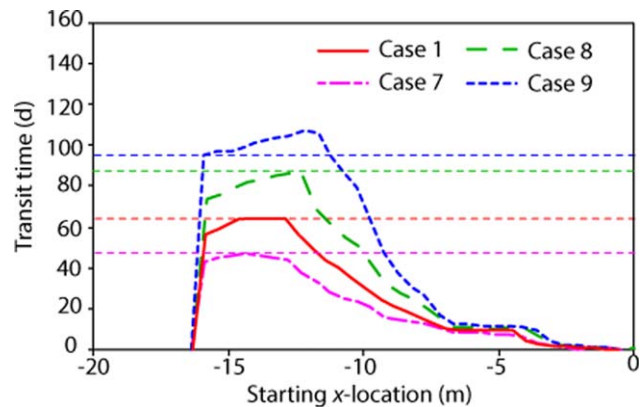
Figure 15. Transit times for seawater particles to recirculate through the aquifer, varying with the infiltration x location along the aquifer-ocean interface for simulations with varying Q_f (Cases 1 and 7–9). The horizontal lines denote the time calculated for the mass of salt in the USP to recover to within 10% (dashed line) of the prestorm conditions for each case.
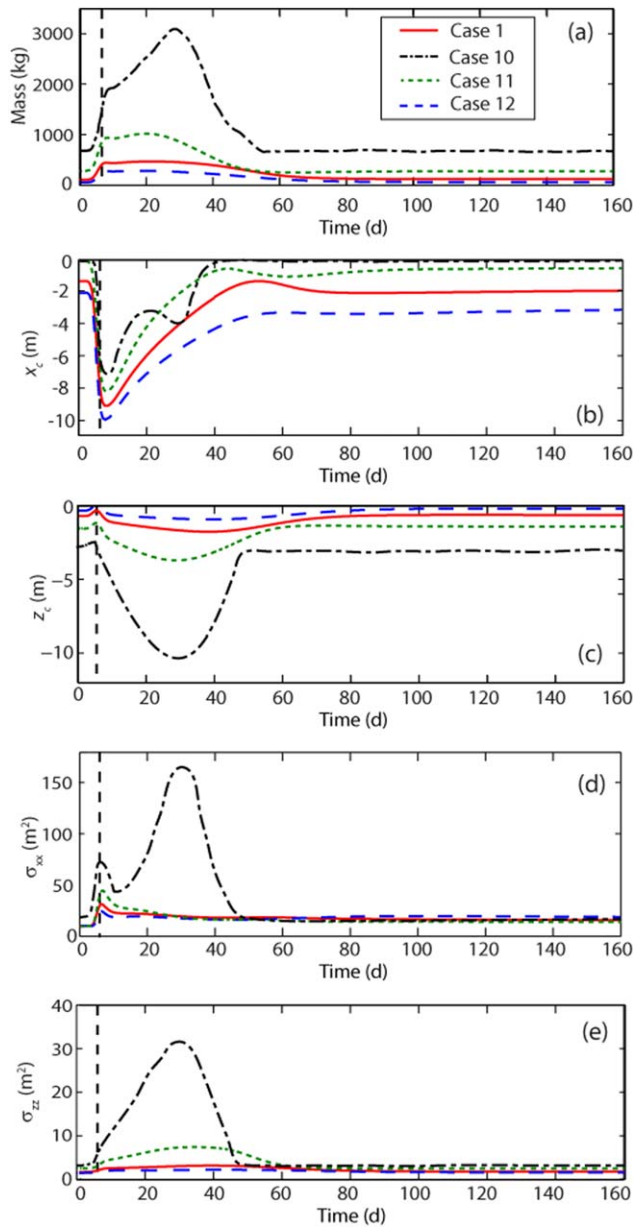
Figure 16. (a) Total salt mass per unit width of aquifer in USP and (b) x coordinate of centroid (x_c), (c) z coordinate of centroid (z_c), (d) horizontal variance (σ_{xx}), and (e) vertical variance (σ_{zz}) of salt in the USP for Case 1 ($K = 10$ m d^{-1}), Case 10 ($K = 50$ m d^{-1}), Case 11 ($K = 21$ m d^{-1}), and Case 12 ($K = 6.7$ m d^{-1}). The time of the storm peak (6 days) is indicated by the vertical black dashed line.

the wave event increased and for all cases corresponded well with the maximum advective transit times of saltwater particles (Figure 6b). Due to the deeper wave-induced seawater recirculation and expanded USP, the interface of the saltwater wedge near the freshwater discharge zone was pushed slightly further seaward as the duration of the wave event increased. This was evident from the spatial moments calculated for the lower domain where the decrease in total salt mass and shift in x_c were greater for the longer wave event. For example, for Case 1 ($F = 2$ days) the total salt mass in the lower aquifer domain decreased by 235 kg m^{-1}

and x_c moved by 0.25 m in the seawater direction compared with a 42 kg m^{-1} salt mass decrease and 0.04 m seaward shift in x_c for Case 6 ($F = 0.5$ days).

3.4. Effect of Freshwater Discharge Rate

[31] The inland forcing provided by the fresh groundwater flux (Q_f) dampened the impact of the wave event on the nearshore salt transport but for the conditions simulated, it did not significantly affect the storm-induced water and salt fluxes across the aquifer-ocean interface. The water influx and efflux across the aquifer-ocean interface for Case 1 ($Q_f = 2.1$ m^3 d^{-1} m^{-1}), Case 7 ($Q_f = 3.15$ m^3 d^{-1} m^{-1}), Case 8 ($Q_f = 1.4$ m^3 d^{-1} m^{-1}), and Case 9 ($Q_f = 1$ m^3 d^{-1} m^{-1}) are shown in Figure 13. For the initial conditions, the net flux was equal to Q_f, and so the water efflux and net flux were less for the cases with reduced Q_f (Cases 8 and 9). The initial influxes were slightly higher for Cases 8 and 9 because the reduced freshwater discharge restricted less the wave- and density-induced seawater recirculation. For the conditions simulated, the influx rates responded similarly to the event; the total storm-induced water influx was only slightly greater for the cases with lower fresh groundwater discharge (18.1 m^3 d^{-1} m^{-1} for Case 7, cf. 23.2 m^3 d^{-1} m^{-1} for Case 9; Table 1).

[32] The fresh groundwater discharge had a greater effect on the salt distribution in the aquifer than the water and salt exchange rates. As expected the USP was initially (prestorm) larger for the simulations with lower fresh groundwater discharge (Figure 14a, Cases 8 and 9). As a counterbalance to the upper seawater recirculation, the increased fresh groundwater flux pushed back the wave-induced recirculation and thus the USP. Due to the reduced resistance to seawater recirculation, the USP expanded more in Cases 8 and 9 compared with Case 1 (Table 1 and Figure 14). For Case 9, the mass of salt in the USP was greatest at ~43 days, and the depth of the plume was greatest at ~61 days. This was delayed compared to the cases with higher Q_f due to the deeper flow paths and slower transport (advective) of recirculating saltwater particles.

[33] The time for the salt mass in the upper aquifer to return to within 10% (surplus) of the prestorm conditions was 46 days for Case 7, 62 days for Case 1, 88 days for Case 8, and 92 days for Case 9. Again the longer recovery period for the cases with reduced Q_f was linked with deeper (and longer) flow paths of the recirculating seawater. Also, once entrained in the fresh groundwater streamlines the velocity of the discharging saltwater particles was less for simulations with lower Q_f. The transit times for the discharging freshwater particles increased for the cases with reduced Q_f, and the flow paths of the shallow freshwater particles were more perturbed for Cases 8 and 9 compared with Cases 1 and 7. The transit times for saltwater particles recirculating through the system for the different cases are shown in Figure 15a. With the exception of Case 9 there was a strong correlation between the maximum transit times and the 10% recovery time. For Case 9, the maximum advective transit time for recirculating saltwater particles was longer (108 days) than the 10% recovery time (96 days). Despite this, at the end of the simulation (160 days) there was still 5.5% of surplus salt remaining in the aquifer relative to the prestorm conditions. This suggests that the dispersive transport and associated fresh-saltwater
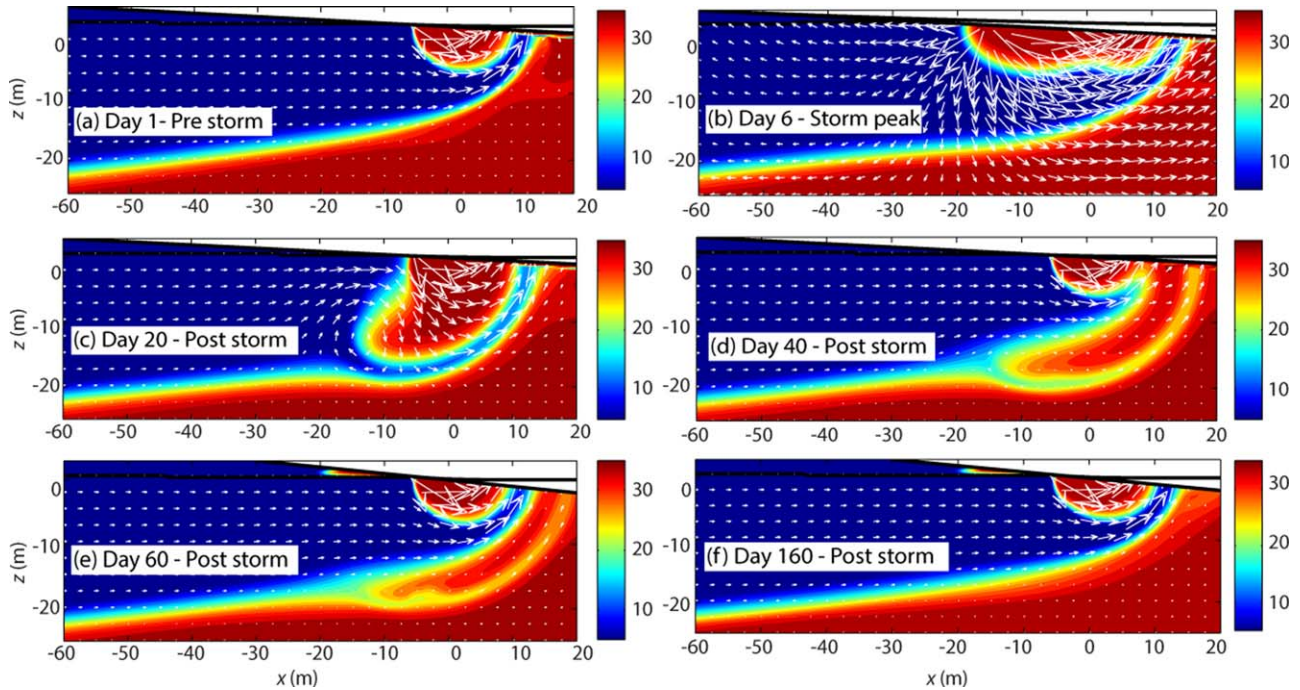
Figure 17. Instantaneous salt concentration (color bars are salinity in ppt) and flow velocities (vectors) for Case 10 ($K = 50$ m d^{-1}). The elapsed times are given in the figure legends. The black lines indicate the wave setup and water table elevation.

mixing may become more important as the advective forcing in the aquifer (driven by the fresh groundwater flux) decreases.

3.5. Effect of Hydraulic Conductivity

[34] The hydraulic conductivity (K) of the aquifer significantly altered the storm-driven fluxes across the aquifer-ocean interface and the nearshore flow and salt transport. The total storm-induced seawater influx increased from 12.2 to 54.1 m^3 m^{-1} as K increased from 6.67 (Case 12) to 50 m d^{-1} (Case 10; Table 1). Consistent with the influx rates, the storm-induced change in the USP salt mass was much greater for the cases with higher K (282 kg m^{-1} for Case 12, cf. 2412 kg m^{-1} for Case 10, Figure 16a). The initial horizontal expansion of the USP was similar for all cases (as indicated by the USP x-centroid location) but higher K led to deeper wave-induced flow recirculation and thus deeper expansion of the USP (Figures 16b and 16c). For Case 10, the USP became sufficiently large that it merged with the saltwater wedge and pushed its interface seaward (Figures 17c and 17d). After the storm receded, the initial freshwater discharge zone re-formed as the freshwater streamlines returned to prestorm conditions and forced the fresh groundwater to discharge near the shoreline (Figures 17d and 17e). The complex nearshore salt distribution for Case 10 led to different behavior of the USP plume centroid and mixing after 20 days compared to the cases with lower K (Figure 16). Although the storm-induced change in USP salt mass increased as K increased (Figure 16), the 10% recovery time decreased to 38 days when $K = 50$ m d^{-1} (Case 10). This indicates that despite the larger disturbance, the salt distribution will return more rapidly to prestorm conditions in coarse sand and gravel beach aquifers. The variances calculated for the USP (Figures 16d and 16e) suggest that the salt-freshwater mixing induced by a wave event will be greater in a more permeable aquifer. It should be noted that although only isotropic conditions were examined, anisotropy ratios (K_x/K_z) in beach aquifers up to 50 are not uncommon [Urish, 2004]. It is expected anisotropy (reduced K_z) would decrease the depth of the wave-induced flow circulations, and this would in turn limit the downward expansion of the USP over the wave event and subsequently the salt-freshwater mixing.

3.6. Effect of Beach Slope (β)

[35] The beach slope controls the width of the wave setup zone, and as a result, the width of the wave-induced recirculations and USP, in addition to the horizontal excursion of the shoreline over the wave event. Simulations performed for steep to mildly sloped beaches ($\beta = 0.1$ in Case 1, $\beta = 0.075$ in Case 13, and $\beta = 0.05$ in Case 14) show that the influence of β on the storm-induced exchange rates across the aquifer-ocean interface is nonmonotonic. The instantaneous and total storm-driven water influx was highest for the case with intermediate beach slope (Case 13, Table 1). As the beach steepens, the excursion of the shoreline over the wave event is reduced, and therefore, there is less area (potential) for seawater infiltration. In contrast, as the beach flattens, although the horizontal shoreline excursion over the wave event is greater, the onshore pressure gradient that drives infiltration is reduced, and as a result there is less influx of seawater into the aquifer. However, the effect of β is small relative to the factors explored above: total storm-driven influx varied only from 20.2 m^3 m^{-1} for Case 1, 23.8 m^3 m^{-1} for Case 13, and 22.2 m^3 m^{-1} for Case 14. Consistent with the total water influxes,
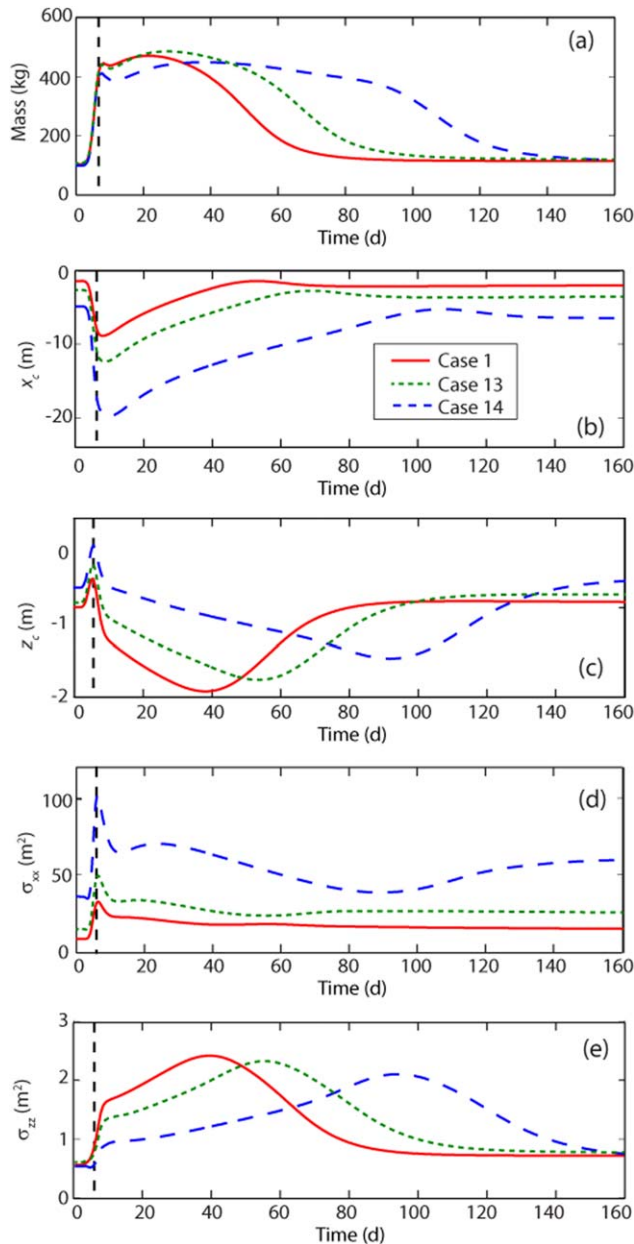
Figure 18. (a) Total salt mass per unit width of aquifer in USP and (b) x coordinate of centroid (x_c), (c) z coordinate of centroid (z_c), (d) horizontal variance (σ_{xx}), and (e) vertical variance (σ_{zz}) of salt in the USP for Case 1 ($\beta = 0.1$), Case 13 ($\beta = 0.075$), and Case 14 ($\beta = 0.05$). The time of the storm peak (6 days) is indicated by the vertical black dashed line.

the change in USP salt mass due to the wave event was similar for all cases and slightly higher for Case 13 (Table 1 and Figure 18a). Despite this, the time for the mass in the USP plume to return to within 10% (surplus) of the prestorm conditions significantly increased as the beach flattened (131 days for Case 14, 86 days for Case 13, and 62 days for Case 1, Figure 18a). The increase in recovery time is caused by longer transport pathways and thus recirculating seawater transit times due to the greater shoreline excursion. In addition, the milder beach slope limits the

beach's drainage capacity following the wave event. The larger shoreline excursion for Case 14 also led to the greatest horizontal shift (landward) in the centroid of the USP and greatest horizontal spreading of the plume (Figures 18b and 18d). The downward expansion of the USP is reduced and more gradual for Case 14 due to the shallower and wider wave-induced recirculation (Figures 18c and 18e).

4. Conclusions

[36] Numerical simulations revealed that intensified wave conditions generated by an offshore storm greatly perturb the flow and salt transport in a subterranean estuary. The seawater influx to a nearshore aquifer was also shown to significantly increase during a wave event. This may lead to large influxes of chemical species such as oxygen, organic matter, and nutrients to a subterranean estuary. The increased availability of these chemicals combined with enhanced wave-induced salt-freshwater mixing may alter the geochemical conditions in a subterranean estuary including the stability of geochemical zonations. In turn this may affect the fate of chemicals discharging and recirculating through a nearshore aquifer. The water efflux also increased in response to the intensified wave conditions. While this increase was caused by higher seawater recirculation rates, it would modify temporal SGD patterns and hence loading rates of chemical species to the sea.

[37] Although wave events of larger magnitude (wave height) and/or longer duration cause greater disturbances to the nearshore salinity distribution and exchange fluxes, a small increase in wave height has the potential to affect processes in a subterranean estuary particularly for nearshore aquifers of higher permeability and with lower fresh groundwater flux. The simulations showed that while exchange fluxes and groundwater flow patterns return to prestorm conditions relatively quickly, it may take up to the order of months for the salinity distribution in a nearshore aquifer to recover. As small wave events occur frequently along coastlines, the next wave event may occur before the aquifer has recovered. This will result in a complex and dynamic salt distribution that is controlled by the combined frequency and magnitude of these events. The increase in wave height was shown to more significantly impact the nearshore aquifer dynamics and aquifer recovery time than the duration of the wave event. For shorter duration events, especially when the beach is flatter and the beach aquifer is less permeable, the depth of the storm-induced seawater recirculation and vertical expansion of the USP are limited to the shallow aquifer sediments.

[38] Previous field investigations of nearshore aquifer dynamics and/or SGD often draw conclusions from single monitoring events. The long recovery times revealed here indicate that analyses need to consider the oceanic forcing conditions in the months leading up to a monitoring event. The results also highlight the need for long-term continuous monitoring at field sites. Only single synthetic wave events were considered here. Simulations considering real time series of wave height over long continuous periods would provide further insight into the dynamic response of the aquifer to long-term varying wave conditions. Understanding the variability induced by changing wave conditions is needed to understand the complexity of the

processes occurring in a subterranean estuary. This complexity will be further increased by nonplanar beach slopes, aquifer heterogeneities, and the interplay with, for example, complex tidal forcing (including spring-neap signal) and seasonal fresh groundwater flux variations. These additional factors and processes should be examined in future investigations to further explore the complexity of the coastal groundwater system, as revealed in this study.

References

Abarca, E., H. Karam, H. F. Hemond, and C. F. Harvey (2013), Transient groundwater dynamics in a coastal aquifer: The effects of tides, the lunar cycle, and the beach profile, *Water Resour. Res.*, *49*, 2473–2488, doi:10.1002/wrcr.20075.

Anschutz, P., T. Smith, A. Mouret, J. Deborde, S. Bujan, D. Poirier, and P. Lecroart (2009), Tidal sands as biogeochemical reactors, *Estuarine Coastal Shelf Sci.*, *84*(1), 84–90, doi:10.1016/j.ecss.2009.06.015.

Appelo, C. A. J. (1994), Cation and proton exchange, pH variations, and carbonate reactions in a freshening aquifer, *Water Resour. Res.*, *30*(10), 2793–2805, doi:10.1029/94WR01048.

Bakhtyar, R., D. A. Barry, and A. Brovelli (2012), Numerical experiments on interactions between wave motion and variable-density coastal aquifers, *Coastal Eng.*, *60*(1), 95–108, doi:10.1016/j.coastaleng.2011.09.001.

Bakhtyar, R., A. Brovelli, D. A. Barry, C. Robinson, and L. Li (2013), Transport of variable-density solute plumes in beach aquifers in response to oceanic forcing, *Adv. Water Resour.*, *53*, 208–224, doi:10.1016/j.advwatres.2012.11.009.

Boufadel, M. C. (2000), A mechanistic study of nonlinear solute transport in a groundwater-surface water system under steady state and transient hydraulic conditions, *Water Resour. Res.*, *36*(9), 2549–2565, doi:10.1029/2000WR900159.

Brovelli, A., X. Mao, and D. A. Barry (2007), Numerical modeling of tidal influence on density-dependent contaminant transport, *Water Resour. Res.*, *43*, W10426, doi:10.1029/2006WR005173.

Burnett, W. C., H. Bokuniewicz, M. Huettel, W. S. Moore, and M. Taniguchi (2003), Groundwater inputs to the coastal zone, *Biogeochemistry*, *66*(1–2), 3–33, doi:10.1023/B:BIOG.0000006066.21240.53.

Carsel, R. F., and R. S. Parrish (1988), Developing joint probability distributions of soil water retention characteristics, *Water Resour. Res.*, *24*(5), 755–769, doi:10.1029/WR024i005p00755.

Cartwright, N., L. Li, and P. Nielsen (2004), Response of salt-freshwater interface in a coastal aquifer to a wave-induced groundwater pulse: Field observations and modelling, *Adv. Water Resour.*, *27*(3), 297–303, doi:10.1016/j.advwatres.2003.12.005.

Charette, M. A., E. R. Sholkovitz, and C. M. Hansel (2005), Trace element cycling in a subterranean estuary. Part 1: Geochemistry of the permeable sediments, *Geochem. Cosmochim. Acta*, *69*(8), 2095–2109, doi:10.1016/j.gca.2004.10.024.

Diersch, H. J., and O. Kolditz (2002), Variable-density flow and transport in porous media: approaches and challenges, *Adv. Water Resour.*, *25*(8–12), 899–944, doi:10.1016/S0309-1708(02)00063-5.

Hays, R. L., and W. J. Ullman (2007), Dissolved nutrient fluxes through a sandy estuarine beachface (Cape Henlopen, Delaware, U.S.A.): Contributions from fresh groundwater discharge, seawater recycling, and diagenesis, *Estuarine Coasts*, *30*(4), 710–724, doi:10.1007/BF02841967.

Johannes, R. E. (1980), The ecological significance of the submarine discharge of groundwater, *Mar. Ecol. Prog. Ser.*, *3*, 365–373.

Kroeger, K. D., and M. A. Charette (2008), Nitrogen biogeochemistry of submarine groundwater discharge, *Limnol. Oceanogr. Methods*, *53*(3), 1025–1039, doi:10.4319/lo.2008.53.3.1025.

Kuan, W. K., G. Jin, P. Xin, C. Robinson, B. Gibbes, and L. Li (2012), Tidal influence on seawater intrusion in unconfined coastal aquifers, *Water Resour. Res.*, *48*, W02502, doi:10.1029/2011WR010678.

Lenkopane, M., A. D. Werner, D. A. Lockington, and L. Li (2009), Influence of variable salinity conditions in a tidal creek on riparian groundwater flow and salinity dynamics, *J. Hydrol.*, *375*(3–4), 536–545, doi:10.1016/j.jhydrol.2009.07.004.

Li, L., and D. A. Barry (2000), Wave-induced beach groundwater flow, *Adv. Water Resour.*, *23*(4), 325–337.

Li, L., D. A. Barry, C. B. Pattiaratchi, and G. Masselink (2002), BeachWin: modelling groundwater effects on swash sediment transport and beach profile changes, *Environ. Model. Software*, *17*(3), 313–320, doi:10.1016/S1364-8152(01)00066-4.

Li, L., N. Cartwright, P. Nielsen, and D. Lockington (2004), Response of coastal groundwater table to offshore storms, *China Ocean Eng.*, *18*(3), 423–431.

Longuet-Higgins, M. S. (1983), Wave set-up, percolation and undertow in the surf zone, *Proc. R. Soc. London, Ser. A*, *390*(1799), 283–291, doi:10.1098/rspa.1983.0132.

Loveless, A. M., and C. E. Oldham (2010), Natural attenuation of nitrogen in groundwater discharging through a sandy beach, *Biogeochemistry*, *98*(1–3), 75–87, doi:10.1007/s10533-009-9377-x.

Mango, A. J., M. W. Schmeeckle, and D. J. Furbish (2004), Tidally induced groundwater circulation in an unconfined coastal aquifer modeled with a Hele-Shaw cell, *Geology*, *32*(3), 233–236, doi:10.1130/G19922.1.

Mao, X., P. Enot, D. A. Barry, L. Li, A. Binley, and D.-S. Jeng (2006), Tidal influence on behaviour of a coastal aquifer adjacent to a low-relief estuary, *J. Hydrol.*, *327*(1–2), 110–127, doi:10.1016/j.jhydrol.2005.11.030.

Masselink, G., and A. D. Short (1993), The effect of tide range on beach morphodynamics and morphology: A conceptual beach model, *J Coastal Res.*, *9*(3), 785–800.

Moore, W. S. (1999), The subterranean estuary: A reaction zone of ground water and sea water, *Mar. Chem.*, *65*(1–2), 111–125, doi:10.1016/S0304-4203(99)00014-6.

Nielson, P. (2009), *Coastal and Estuarine Processes, Advanced Series on Ocean Engineering*, vol. 29, World Sci., Singapore.

Robinson, C., B. Gibbes, and L. Li (2006), Driving mechanisms for flow and salt transport in a subterranean estuary, *Geophys. Res. Lett.*, *33*, L03402, doi:10.1029/2005GL025247.

Robinson, C., B. Gibbes, H. Carey, and L. Li (2007a), Salt-freshwater dynamics in a subterranean estuary over a spring-neap tidal cycle, *J. Geophys. Res.*, *112*, C09007, doi:10.1029/2006JC003888.

Robinson, C., L. Li, and D. A. Barry (2007b), Effect of tidal forcing on a subterranean estuary, *Adv. Water Resour.*, *30*(4), 851–865, doi:10.1016/j.advwatres.2006.07.006.

Robinson, C., A. Brovelli, D. A. Barry, and L. Li (2009), Tidal influence on BTEX biodegradation in sandy coastal aquifers, *Adv. Water Resour.*, *32*(1), 16–28, doi:10.1016/j.advwatres.2008.09.008.

Shand, T. D., I. D. Goodwin, M. A. Mole, J. T. Carley, S. Browning, I. G. Coghlan, M. D. Harley, W. L. Peirson, Z. J. You, and M. A. Kulmar (2010), NSW Coastal storms and extreme waves, paper presented at 19th NSW Coastal Conference, Australian Coastal Society, Batemans Bay, New South Wales.

Slomp, C. P., and P. van Cappellen (2004), Nutrient inputs to the coastal ocean through submarine groundwater discharge: controls and potential impact, *J. Hydrol.*, *295*(1–4), 64–86, doi:10.1016/j.jhydrol.2004.02.018.

Smith, A. J. (2004), Mixed convection and density-dependent seawater circulation in coastal aquifers, *Water Resour. Res.*, *40*, W08309, doi:10.1029/2003WR002977.

Spiteri, C., P. Regnier, C. P. Slomp, and M. A. Charette (2005), pH-dependent iron oxide precipitation in a subterranean estuary, *J. Geochem. Explor.*, *88*(1–3), 399–403, doi:10.1016/j.gexplo.2005.08.084.

Spiteri, C., C. Slomp, K. Tuncay, and C. Meile (2008a), Modeling biogeochemical processes in subterranean estuaries: Effect of flow dynamics and redox conditions on submarine groundwater discharge of nutrients, *Water Resour. Res.*, *44*, W04701, doi:10.1029/2007WR006071.

Spiteri, C., C. P. Slomp, M. A. Charette, K. Tuncay, and C. Meile (2008b), Flow and nutrient dynamics in a subterranean estuary (Waquoit Bay, MA, USA): Field data and reactive transport modeling, *Geochem. Cosmochim. Acta*, *72*(14), 3398–3412, 10.1016/j.gca.2008.04.027.

Urish, D. W. (2004), Determination of the temporal and spatial distribution of beach face seepage, in *Coastal Aquifer Management: Monitoring, Modelling and Case Studies*, edited by A. H. D. Cheng and D. Ouzar, pp. 143–165, Lewis Publ., New York.

van Genuchten, M. T. (1980), A closed form equation for predicting the hydraulic conductivity of unsaturated soils, *Soil Sci. Soc. Am. J.*, *44*(5), 892–898, doi:10.2136/sssaj1980.03615995004400050002x.

Voss, C., and W. Souza (1987), Variable density flow and solute transport simulation of regional aquifers containing a narrow freshwater-saltwater transition zone, *Water Resour. Res.*, *23*(10), 1851–1866, doi:10.1029/WR023i010p01851.

Voss, C. I., and A. M. Provost (2002), A model for saturated-unsaturated variable-density groundwater flow with solute or energy transport, *Water Res. Invest. Rep. 02–4231*, U.S. Geol. Surv., Reston, Va.

Werner, A. D., M. Bakker, V. E. A. Post, A. Vandenbohede, C. Lu, B. Ataie-Ashtiani, C. T. Simmons, and D. A. Barry (2013), Seawater intrusion processes, investigation and management: Recent advances and future challenges, *Adv. Water Resour.*, *51*, 3–26, doi:10.1016/j.advwatres.2012.03.004.

Westbrook, S. J., J. L. Rayner, G. B. Davis, T. P. Clement, P. L. Bjerg, and S. J. Fisher (2005), Interaction between shallow groundwater, saline surface water and contaminant discharge at a seasonally and tidally forced estuarine boundary, *J. Hydrol.*, *302*(1–4), 255–269, doi:10.1016/j.jhydrol.2004.07.007.

Xin, P., C. Robinson, L. Li, D. A. Barry, and R. Bakhtyar (2010), Effects of wave forcing on a subterranean estuary, *Water Resour. Res.*, *46*, W12505, doi:10.1029/2010WR009632.